Ultrafast Entropy Production and Markovianity in Nonequilibrium Magnets

Finja Tietjen[1], R. Matthias Geilhufe[1]

[1]*Department of Physics, Chalmers University of Technology, Gothenburg, SE*

INTRODUCTION: This contribution is based on Ref. [1]. Manipulation of magnetic degrees of freedom is central for nanotechnology and spintronics. Ultrafast dynamics involve demagnetization, switching, and magnonic effects, tied to entropy production motivating ultrafast thermodynamics. These nonequilibrium processes are naturally described by stochastic thermodynamics, which extends entropy concepts microscopically and to collective excitations [2]. Yet, experimentally accessing entropy production remains difficult. Here, we derive it in laser-driven magnets, including nutation, and compare theory with MOKE experiments [3]. Furthermore, we use entropy production rates for different versions of the magnetization dynamics to investigate their Markovianity.

METHODS: We are using an extend verison of the Landau-Lifshitz-Gilbert equation as the starting point. It describes the ultrafast precession, nutation, damping and fluctuations of magnetization after a laser pulse. By applying the path-integral formalism, we obtain the entropy production rate analytically.

To verify the results, we simulate trajectories of magnetization based on experimental data and calculate the entropy production for different materials.

Different magnetization dynamics – with and without nutation, and based on quantum mechanics or classical mechanics – are simulated as well. Then their entropy production rates are calculated and compared [4].

RESULTS: We show that the entropy production rate can be calculated by means of ultrafast thermodynamics and that we can match experimental results.

This opens up a possibility to measure entropy.

Knowing the entropy production rates, which can be obtained from the entropy production itself, gives information about the Markovianity of the underlying dynamics.

DISCUSSION & CONCLUSIONS: Not only can entropy production be calculated for magnetization dynamics from ultrafast thermodynamics, but the entropy production rates are a reliable measure for the Markovianity of the dynamics.

ACKNOWLEDGEMENTS: This template was modified with kind permission from eCM conferences Open Access online periodical & eCM annual conferences. The work on Markovianity is conducted in collaboration with Felix Hartman and Janet Anders from University of Potsdam.

REFERENCES:

[1] Tietjen F, Geilhufe RM. 2025. Ultrafast entropy production in nonequilibrium magnets. PNAS Nexus 4, pgaf055

[2] Caprini L, Löwen H, Geilhufe RM. 2024. Ultrafast entropy production in pump-probe experiments. Nat Commun. 15(1):94.

[3] Neeraj K, et al. 2021. Inertial spin dynamics in ferromagnets. Nat Phys. 17(2):245–250.

[4] Hartman F, Tietjen F, Geilhufe RM, Anders J. 2025. Entropy production for investigation of extended Landau-Lifshitz-Gilbert equation. *Submitted.*

Reinforcing Conjugated Polymers with Nanocellulose

Jan Jacobs[1,2], Zhu Di[1], Mohammad Morsali[1,2], Judith Pons i Tarrés[1], Joost Kimpel[1], Mariavittoria Craighero[1], Meghna Jha[1], Shuichi Haraguchi[1] and Christian Müller[1,2]

[1]*Department of Chemistry and Chemical Engineering, Chalmers University of Technology, 41296 Göteborg, Sweden*
[2]*Wallenberg Wood Science Center, Chalmers University of Technology, 41296 Göteborg, Sweden*

Conjugated polymers are in high demand for a wide range of applications from wearable electronics to bioelectronics. While the optimization of their electrical properties is increasingly well understood, the design of materials with balanced mechanical properties has received less attention. One way to adjust the stiffness of a conjugated polymer is through the addition of a filler, such as cellulose nanofibrils. Many conjugated polymers with a state-of-the-art electrical performance are processable from organic solvents, while cellulose nanofibrils are typically processed from water. This solvent mismatch complicates compounding from solution.

Here, the preparation of nanocomposites through in-situ polymerization is presented. Direct arylation polymerization is used to prepare a thienothiophene-based copolymer in the polar solvent N-butyl-2-pyrrolidone, which also contains dispersed cellulose nanofibrils. After removal of the solvent, which acted as both the reaction and dispersion medium, a fine composite is obtained. Considerable reinforcement is observed, as evidenced by an increase in elastic modulus from about 0.2 GPa for the neat polymer to more than 1.1 GPa for a dry composite containing 15 vol% cellulose nanofibrils. The stiffness of composites could be reversibly reduced by at least 50% through water uptake, enabling the design of organic semiconducting materials with switchable mechanical properties.

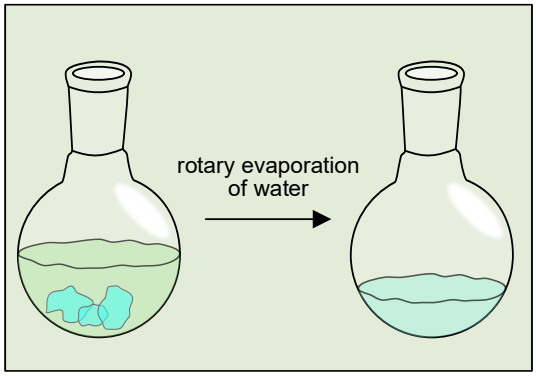

solvent exchange of CNF Hydrogel
from water to high boiling point organic solvent

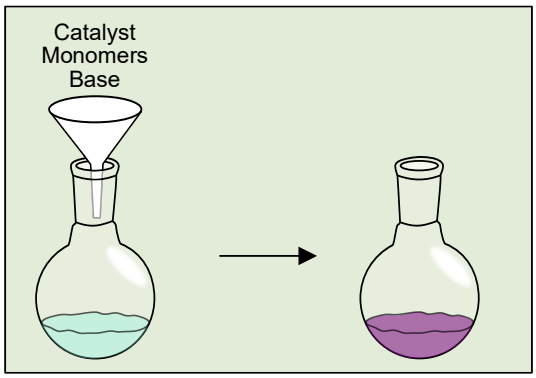

in-situ direct arylation polymerization
of polythiophene

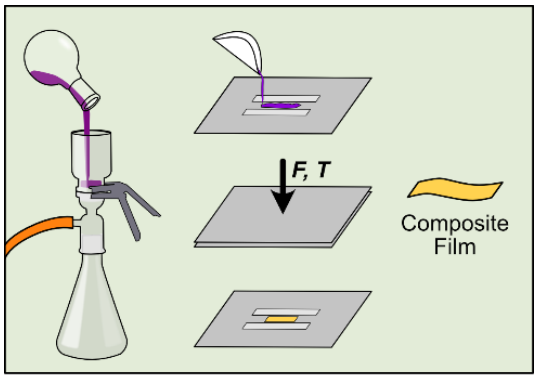

Filtration and hot pressing of composite material

Figure 1: Synthesis of conductive polymer/cellulose nanofibril composites

Plasma Surface Engineering of Graphite and Its Effect on Advancing the Performance of Aluminium Battery

Ruiqi Chen[1], Neelakandan M. Santhosh[2], Komal Gola[1], Nitish Kumar[1], Uroš Cvelbar[2], Jinhua Sun[1]

[1]*Department of Industrial and Materials Science, Chalmers University of Technology, Göteborg, SE-412 96, Sweden*

[2]*Department of Gaseous Electronics (F6), Jožef Stefan Institute, Jamova 39, Ljubljana SI-1000, Slovenia*

INTRODUCTION: Aluminium batteries, with high gravimetric capacities and cost-effective aluminium metal anodes, are a promising alternative to the existing energy storage devices. Among variously explored cathode active materials, graphite is a front runner due to its high electrical conductivity and the capability to accommodate chloroaluminate anions for non-aqueous aluminium batteries. However, the quality of graphite, surface chemistry, contamination, and various structures affect the performance differently.

METHODS: A mild hydrogen and argon plasma was used to engineer the graphite surface and tailor the structural quality to investigate their effect on the storage capabilities of chloroaluminate anions [1]. The electrochemical behaviour of graphite and plasma-treated graphite as cathode materials was evaluated in a standard Swagelok cell using aluminium as anode and an ionic liquid mixed with 1-ethyl-3-methylimidazole hydrochloride and anhydrous aluminium chloride as the electrolyte.

RESULTS: By tailoring the surface characteristics of graphite with hydrogen plasma, the most favourable graphite configuration was optimized and tested for aluminium battery. The hydrogen plasma-treated graphite structures show higher capacity by delivering 132.68 mAh/g at a current density of 50 mA/g and demonstrate excellent stability over cycling for 1000 cycles by maintaining 98% of initial capacity at a high current density of 500 mA/g (Fig. 1).

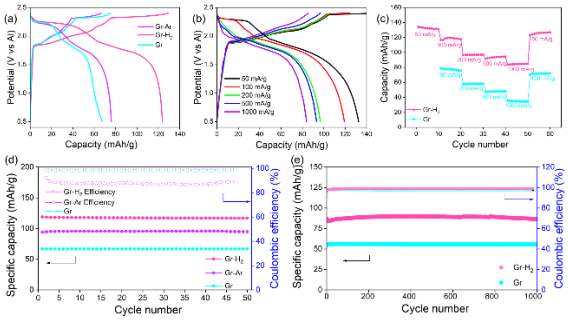

Fig. 1: Electrochemical performance of plasma treated graphite as cathode for aluminium battery.

DISCUSSION & CONCLUSIONS: Our results provide a useful perspective for developing surface modification of graphite for high-performance aluminium batteries. The proposed plasma treatment strategy holds a promising route for integration into industrial electrode fabrication with its simplicity and compatibility with existing battery manufacturing processes.

ACKNOWLEDGEMENTS: This work was supported by the EU Graphene Flagship FLAG-ERA III JTC 2021 project "VEGA" (2021-05924, ANR-21-GRF1-0004 or MIZS-PR-11938), Chalmers Area of Advance-Production, 2D TECH VINNOVA competence Centre (2019-00068).

REFERENCES:

[1] R. Chen, N. M. Santhosh, J. Zavašnik, R. K. Trivedi, S. Joseph, K. Gola, N. Kumar, U. Cvelbar, J. Sun, Carbon, (2025) Pages 120835, Plasma Surface Engineering of Graphite and its Effect on Advancing the Performance of Aluminium Battery, DOI: https://doi.org/10.1016/j.carbon.2025.120835.

Electro-Chemo-Mechanical Coupling in Structural Lithium-Ion Batteries: Experimental Findings and Numerical Modelling

R. Al-Emrani[1], C. Larsson[1], C. Dahlberg[1], F. Larsson[1], L.E. Asp[1], J. Xu[1]

[1]*Division of Material and Computational Mechanics, Department of Industrial and Material Science, Chalmers University of Technology*

INTRODUCTION: Structural battery composites combine electrical and mechanical functionalities into a single laminate. In structural batteries, carbon fibres (CF) are a central component, as they can store lithium and act as both mechanical reinforcement and current collector. Similarly, $LiFePO_4$ (LFP) used in the positive electrode, hosts lithium and provides mechanical stiffening. These combined functionalities give rise to the electro-chemo-mechanical coupling effect. In this work we aim to define and quantify this coupling effect for a discharged cell, implementing an experimental-computational framework for structural battery full cells with a carbon fibre negative electrode and a commercial LFP-based positive electrode.

METHODS: During the experimental work, the voltage-strain coupling effect was studied by placing the cell into a tensile machine and measuring the open-circuit potential during cyclic mechanical loading. To implement the experiment numerically, an electro-chemo-mechanical model is considered where the fields are coupled over the different domains [1]. The chemo-mechanical coupling is given by the highlighted coupling terms for the mechanical stresses, $\boldsymbol{\sigma}$, and the chemical potential, μ_{Li}^{en}, according to

$$\boldsymbol{\sigma}(\boldsymbol{\epsilon}, c_{Li}) = \mathbb{E}(c_{Li}) : \left[\boldsymbol{\epsilon} - \boldsymbol{\alpha}_i \frac{c_{Li} - c_{Li}^0}{\tilde{c}_i}\right] \qquad [1]$$

$$\mu_{Li}^{\mathrm{en}}(\boldsymbol{\epsilon}, c_{Li}) = -\frac{1}{\tilde{c}_i}\boldsymbol{\alpha}_i : \boldsymbol{\sigma} + \mu_i^0 + RT\ln\left(\frac{c_{Li}}{\tilde{c}_i - c_{Li}}\right) + \frac{\mathrm{d}}{\mathrm{d}c_{Li}}\Lambda(c_{Li}, \tilde{c}_{CF} - c_{Li}) \, . \qquad [2]$$

In Eq. [1] the highlighted term describes the chemical strains which influence the mechanical stresses while the term in Eq. [2] shows how the chemical potential is influenced by the mechanical stresses. The coupling effect is studied in the model by investigating the contribution for both electrodes, each electrode separately and comparing the obtained data to the experimental results.

RESULTS: Figure 1 shows the normalised potential over time for the experiment compared to three different numerical cases: when electro-chemo-mechanical coupling is considered for both electrodes, for the negative electrode and for the positive electrode. As seen, the variation in potential when coupling is considered on both electrodes and separately for the negative electrode are almost identical. Additionally, the calculated cell potential correlates well to the measured one, both in amplitude and absolute value. However, when coupling is considered only on the positive electrode the potential is almost constant and deviates from the experiment.

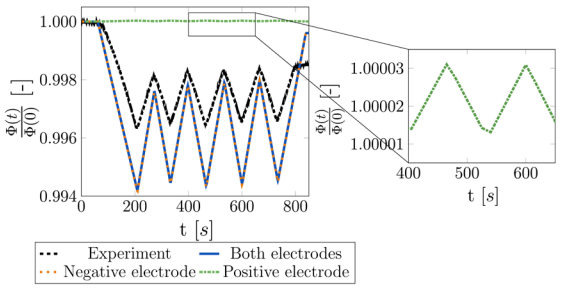

Fig. 1: The calculated electric potential-time curves of the discharged cell compared to the experimental results.

CONCLUSIONS: From the results it is seen that it is the CF in the negative electrode that fully control the voltage-strain coupling effect in structural battery full cells with a commercial positive electrode.

ACKNOWLEDGEMENTS: This work is financially supported by the Swedish Research Council (VR).

REFERENCES: [1] C. Larsson, F. Larsson, J. Xu, K. Runesson, L. E. Asp, Electro-chemo-mechanical modelling of structural battery composite full cells, npj Computational Materials 11 (141) (2025).

Modification of Aluminum Foil as Anode Current Collector for Lithium Ion Battery

H. Badreldin, N. Kumar, R. Chen, J. Sun

Department of Industrial and Materials Science, Chalmers University of Technology, Göteborg, SE-412 96,

INTRODUCTION: With the rapid increase in electrification, the use of copper(Cu) as a current collector in batteries raises concerns about its availability and cost. This project aims to reduce Cu usage at the anode while maintaining excellent conductivity, low thickness and weight.

METHODS: -

Battery-grade aluminium foil was degreased and deoxidized to improve Cu adhesion, then electroless seeded and electroplated in a $CuSO_4$ solution using a DC power supply.

- Layer-by-layer (LbL) deposition of interface materials and graphene was used to achieve a uniform graphene coating on the aluminium substrate.

- A standard graphite electrode was used for all electrochemical testing in a half-cell configuration.

RESULTS: The cycling performance demonstrates a stable capacity of 350 mAh/g over30 cycles, consistent with commercial copper testing. The charge/discharge curve is also consistent with reference tests. CV testing shows an ideal curve with no signs of irregular peaks or side reactions. Further testing and optimization are planned to investigate long-term performance

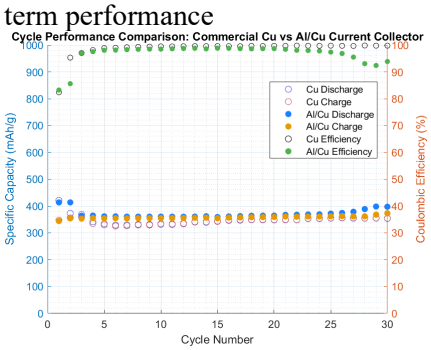

Fig. 1: Cyclic performance using graphite electrode comparing composite current collector and commercial copper foil.

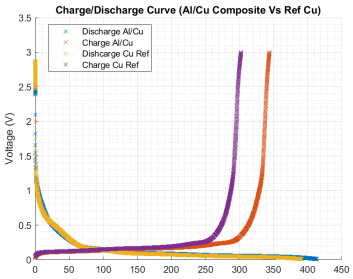

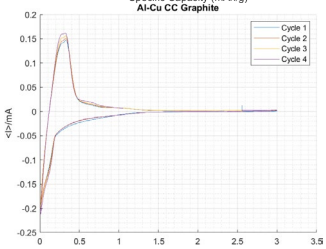

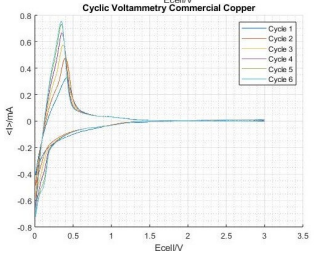

DISCUSSION & CONCLUSIONS: The usage of alternative current collectors provides a solution to increasing energy densities of todays batteries as well as reducing the impact of increasing copper metal prices and demand. This method shows a simple wet effective way to make use of already available materials to fabricate current collectors.

ACKNOWLEDGEMENTS: Area of Advance Production and COMPEL

REFERENCES: -

Pd/CeO_2 Inverse Opals for Electrocatalytic Alkaline HOR

Michael Wilms[1], Ruby S. Raju[1], Deya Sallaberry[1] and Mathilde Luneau[1]*
[1]*Department of Chemistry and Chemical Engineering, Competence Centre for Catalysis, Chalmers University of Technology, Gothenburg, SE 41296, Sweden.*
wilmsm@chalmers.se

INTRODUCTION: Hydrogen fuel cells have emerged as attractive replacements to the highly polluting internal combustion engine with proton exchange membrane fuel cells (PEMFCs) being the most advanced technology which has seen limited commercial uptake. The main drawbacks preventing their widespread adoption are acidic environment induced instability of electrodes and sluggish kinetics of the oxygen reduction reaction at the cathode.[1] This limits the catalyst choice to platinum which constitutes around 40% of total cell cost (includes application).[2]

Anion exchange membrane fuel cells (AEMFCs) have emerged as a promising alternative with a less corrosive cell environment allowing a wider choice of catalysts. However, the switch to alkaline conditions in turn leads to sluggish kinetics in the hydrogen oxidation reaction (HOR) at the anode. It has been suggested that an ideal HOR catalyst balances active sites for both H_{ads} and OH_{ad} which has been scarcely realized with non-Pt catalysts.[3] In this work, butterfly wing inspired porous CeO_2/Pd inverse opal networks were synthesized, which maximize active site accessibility and mass transport. The CeO_2 support functions as an oxyphilic OH^- donor, while metal–support interactions modulate the hydrogen binding energy of palladium[4]

METHODS: The inverse opal structure was fabricated by self-assembling monodisperse polymer microspheres onto a glassy carbon electrode. The template was then infiltrated with Ce and Pd precursors before calcination at 500°C (Fig 1 a). Electrochemical activity was studied using cyclic voltammetry in a standard three-electrode electrochemical cell in a rotating disk electrode (RDE) configuration. CVs were measured in 0.1 M KOH electrolyte at room temperature using a graphite rod as counter electrode and a Hg/HgO reference electrode. Scanning electron microscopy, transmission electron microscopy, x-ray ray photoelectron spectroscopy.

RESULTS: The preparation method yields highly ordered IOs (Fig 1b). The inverse opal structure allows superior diffusion of reactants OH^- and H_2 to electrochemically active sites. The electrochemically active surface area (ECSA) can be finely tuned by modulating the size of the polymer microspheres. In this study, polymer microspheres of size 100, 330 and 500 nm were employed with 100 nm spheres yielding the highest current density at 0.1 V_{RHE} with 10 wt% Pd loading, likely due to the higher surface area and better dispersion of Pd throughout the structure. A peak current density of 0.27 mA/cm^2_{Pd} at 0.1 V_{RHE} in alkaline media was achieved using a 100 nm IO with 10 wt% Pd, 11-fold that of a planar Pd film (Fig 1 c). The electrochemically active surface area (ECSA) was found to decrease with increasing pore size, with an estimated value of 0.04 cm^2 for the 100 nm sample.

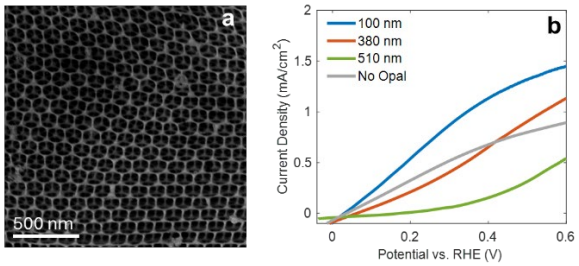

Fig. 1: SEM micrograph of CeO_2/Pd inverse opal film. (c) HOR performed in H_2-saturated 0.1 M KOH at 5 mV s^{-1} and 1600 rpm.

DISCUSSION AND CONCLUSIONS: The reduction in ECSA observed for larger pore sizes highlights the need to balance mass transport within the support material and its conductivity, particularly when using semiconducting supports such as CeO_2. The results demonstrate that scaling the pore size down to the mesoporous regime preserves sufficient conductivity while enhancing both the kinetics and mass transport of the hydrogen oxidation reaction (HOR) in alkaline media.

REFERENCES: [1] H. Cruz-Martínez, et al., *Materials Today Physics* **2021**, 19, 100406.
[2] G. K. Adria Wilson, and Dimitrios Papageorgopoulos, (Ed: U. D. o. Energy), 2017.
[3] D. Strmcnik, et al., *Nat Chem* **2013**, 5, 300.
[4] M. Luneau, et al., *Journal of Materials Chemistry A* **2023**, 11, 16370.

Self-healing, recyclable, and degradable castor oil-based elastomers for sustainable soft robotics

A. Costa Cornellà[1*], G. Van Assche[1], Christian Müller[2] J. Brancart[1]

[1]*Sustainable Materials engineering (SUME), Vrije Universiteit Brussel,* [2] *Department of Chemistry and Chemical Engineering, Chalmers University of Technology*

*Current affiliation: Department of Chemistry and Chemical Engineering, Chalmers University of Technology

INTRODUCTION:.

Conventional polymers used for soft robotics, are fossil-based, they are non-recyclable and prone to damage. In nature, many biological tissues, have the ability to repair themselves after damage, which inspired the development of self-healing polymers. Self-healing polymers render their life cycle more sustainable by recovering their properties upon healing. Intrinsic self-healing polymers can be recycled, which further reduces waste production. Yet, despite these intrinsic benefits, several sustainability issues remain largely neglected in current self-healing materials. In this work[1], we present a series of self-healing elastomers, based on Diels-Alder (DA) bonds, developed with sustainability as the main design parameter. To show its applicability in the soft-robotic fields we used them to fabricate a self-healing multi-material soft gripper.

METHODS:

Castor oil was functionalized through a solvent-less, one-pot synthesis using renewable cyclic anhydrides followed by a reaction with furfuryl glycidyl ether to introduce the furan groups. The materials were then crosslinked with two types of bismaleimides. The obtained networks combined two types of dynamic bonds (DA, and hydrogen bonds). Characterization included FTIR, HNMR, DSC, rheology, and mechanical testing. Initial assessments of recyclability and hydrolytic degradation were also performed.

RESULTS:.

The elastomers have a Young's modulus between 0.5 to 20 MPa, and elongations at break of up to 487%, which covers the range required for soft robotics. The materials showed an efficient self-healing performance at room temperature, up to 75% recovery after 24h. Mechanical properties stayed the same after three recycling cycles. And the materials degraded under accelerated conditions within 8-14 days. By taking advantage of these unique properties, a soft pneumatic gripper capable of healing autonomously after puncture and a full cut damage, regaining its airtightness and functionality.

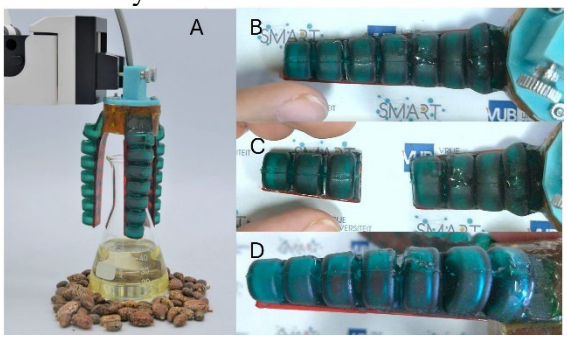

Fig. 1: A. Photo of the gripper on top of an Erlenmeyer flask with castor oil surrounded by castor seeds. B-C. Photos of the damaging and posterior healing of one of the gripper fingers.

DISCUSSION & CONCLUSIONS:

The use of castor oil as the main part of the backbone is key as it does not compete with food, grows fast and it is resistant to pests and drought, yet is not toxic. The process avoids hazardous solvents and follows the 12 principles of green chemistry. The key to designing materials displaying fast and efficient low-temperature self-healing with adequate mechanical strength and stability is the synergistic combination of weak hydrogen bonds and dynamic DA covalent bonds. The former are faster a provide a immediate partial recovery which is key to obtaining a full recovery with the DA bonds. This study demonstrates a holistic approach of sustainable self-healing elastomers, and we aim that our approach provides a model for developing the next generation of materials for soft robotics, but also for other applications that require elastomers.

ACKNOWLEDGEMENTS:

Marie Sklodowska-Curie grant agreement no. 860108 (SMART),

REFERENCES:

1. Costa Cornellà, A. *et al.* Self-healing, recyclable, and degradable castor oil-based elastomers for sustainable soft robotics. *ACS Sustain. Chem. Eng.* **11**, 3437–3450 (2023).

Accounting for B-type carbonate in bone elemental analyses

J. Ewerman[1], F.B.G. Zambardino[1], H. Ben Amara[1], A. Palmquist[1], F.A. Shah[1]
[1]*Department of Biomaterials, Sahlgrenska Academy, University of Gothenburg, Sweden*

INTRODUCTION: Bone extracellular matrix is a nanocomposite material consisting of an organic matrix, mainly collagen type-I, and an inorganic matrix, i.e., bone mineral. The structure and chemical composition of bone mineral is a heavily debated subject and it is often incorrectly labelled as "hydroxy(l)apatite" (HAp) (1). This mislabelling complicates bone mineral characterisation since it places preconceptions on both structural and chemical properties of the mineral, e.g., that the calcium to phosphorous ratio (Ca/P) "should" be ~1.67 (i.e. the stoichiometric value of Ca/P for HAp) in mature bone. As a result, this leads to misinterpretation of experimental data as it ignores the cation and anion substitutions, such as carbonate (CO_3^{2-}) occupying trivalent anionic phosphate (PO_4^{3-}) sites in the apatite crystal lattice (also called B-type substitution) (2). Thereby, bone mineral is better described as an ion-substituted carbonated apatite (1). We present a simple approach towards a realistic measurement of elemental composition of bone mineral by accounting for cation and anion site substitutions (3).

METHODS: Bovine bone slices were commercially sourced (https://boneslices.com) and systematically deproteinised using 5 % NaOCl at 4 °C for up to 168 h. Energy-dispersive X-ray spectroscopy (EDX) was used for elemental analysis. Raman spectroscopy was used to monitor deproteinisation and to enable phosphorus correction based on B-type carbonate substitution. Backscattered electron scanning electron microscopy (BSE-SEM) was used to image the bone slices. One-way analysis of variance (ANOVA) with post hoc Bonferroni correction was used for statistical analysis of the cation-to-anion ratios (CAR) between 0 h, 96 h, and 168 h.

RESULTS: Raman spectroscopy shows a gradual decrease in organic matrix (amide III) in relation to mineral content ($\nu_2PO_4^{3-}$) (**Fig. 1A**), going from undeproteinised (whole bone) to completely deproteinised after 168 h of NaOCl exposure, further validated by inverse mineral-to-matrix ratio (1/MMR) (**Fig. 1B**), and increasing atomic number (*Z*-contrast) on BSE-SEM (**Fig. 1C**). EDX reveals that the CARs (Ca/P, Ca+Mg+Na/P) increase from 0 h to 96 h and 168 h ($p < 0.0001$, $p < 0.0001$), and from 96 h to 168 h ($p < 0.0001$). Additionally, phosphorus correction (P_{corr}) based on Raman spectroscopy tends to decrease the overall CAR values (**Fig. 1D**).

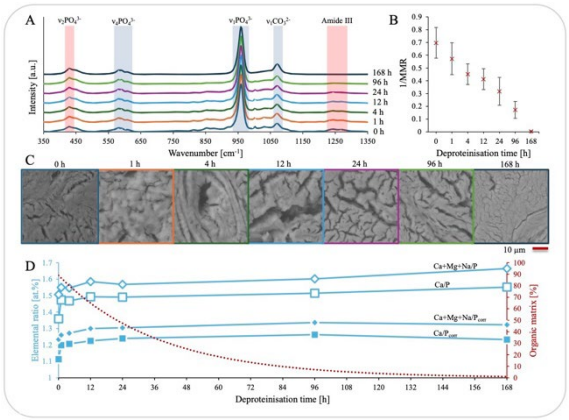

Fig.1: (A) Raman spectra of deproteinised bone (y-shifted and stacked). (B) Inverse MMR mean values (red crosses) and standard deviations (vertical lines). (C) BSE-SEM images. (D) CARs calculated using EDX. Secondary x-axis shows the organic matrix content.

DISCUSSION & CONCLUSIONS: The increase in CAR values using uncorrected phosphorus values over deproteinisation time show that they are strongly influenced by the organic matrix, making whole bone inadequate to use for analysing elemental composition of bone mineral. Additionally, the decrease in CAR values obtained using corrected phosphorous values marks that uncorrected CAR values are grossly overestimated as it ignores the phosphate sites occupied by carbonate ions in the apatite lattice. Correlative EDX and Raman spectroscopy performed on completely deproteinised bone reveals a more realistic view of bone mineral elemental composition by eliminating uncertainties introduced by the organic matrix and accounting for expected cation and anion substitutions.

ACKNOWLEDGEMENTS: Funding from Svenska Sällskapet för Medicinsk Forskning (SSMF), Vetenskapsrådet, the IngaBritt and Arne Lundberg Foundation, the Hjalmar Svensson Foundation, and the Chalmers Materials Analysis Laboratory (CMAL) is acknowledged.

REFERENCES:

1. Wopenka B, Pasteris JD. Mat Sci Eng C. 2005;25.
2. Taylor EA, Mileti CJ, Ganesan S, Kim JH, Donnelly E. Calcif Tissue Int. 2021;109.
3. Shah FA. Acta Biomater. 2025;196.

Inertial Repulsion from Quantum Geometry

M. Fahrensohn[1], R. M. Geilhufe[1]

[1] *Department of Physics, Chalmers University of Technology, 41296 Göteborg, Sweden*

INTRODUCTION: Quantum electrodynamics provides a comprehensive framework for describing the interaction between matter and the electromagnetic field. Local U(1) gauge invariance is enforced through the covariant derivative, which introduces the electromagnetic field as a gauge field. The success of this approach in describing fundamental forces has inspired many subsequent quantum field theories.
Motivated by the growing interest in reciprocal-space geometry, which plays a central role in modern condensed matter physics, we extend this approach to a geometric U(1) gauge symmetry in momentum space. This allows us to investigate the emergence of effective forces from geometric gauge connections in Hamiltonians containing terms that couple linearly to the position operator. Previous studies [1,2] have shown that these terms appear naturally in non-inertial or rotating frames of reference. In particular, for electrons bound to a rotating ion, the Hamiltonian acquires inertial terms that include a linear coupling of the centrifugal force to the position operator [1,2]. By considering these couplings within a reciprocal-space gauge-theory framework, we demonstrate that enforcing local geometric U(1) invariance leads to an emergent, repulsive Coulomb-like interaction in reciprocal space in the non-inertial frame.

METHODS: The main methods used in this project are quantum field theory and gauge theory. Drawing from quantum electrodynamics and modern theories on Berry electrodynamics, we consider terms in the Hamiltonian that couple linearly to the position operator in real space and introduce a covariant derivative in reciprocal space that enforces local geometric U(1) gauge invariance. Upon integrating out the associated gauge field, this formalism leads to emergent interaction terms in the effective Hamiltonian.

RESULTS: The resulting effective, repulsive Coulomb-like interaction is proportional to $1/|\mathbf{k}-\mathbf{k}'|$. In real space, this corresponds to an effective interaction that scales with the inverse square of the distance, leading to a dipole-dipole-like interaction force proportional to $1/|\mathbf{r}|^3$. The magnitude of this force scales with the square of the centrifugal force and therefore depends on the frequency and radius of rotation.
DISCUSSION & CONCLUSIONS: The emergent repulsive interaction shows how non-inertial motion and geometric effects can combine to produce observable dynamical effects. Such effects are expected to contribute corrections to the energy levels of particles in rotating or accelerated frames. The framework here is relevant to a wide variety of systems, from axial phonons and molecular rotation (e.g., in metal-organic frameworks) to astronomical systems such as pulsars, and can be generalized beyond purely rotational motion to accelerated frames of reference.
ACKNOWLEDGEMENTS: We acknowledge support from the Swedish Research Council (VR starting Grant No. 2022-03350), the Olle Engkvist Foundation (Grant No. 229-0443), the Royal Physiographic Society in Lund (Horisont), the Knut and Alice Wallenberg Foundation (Grant No. 2023.0087),
and Chalmers University of Technology, via the department of physics and the Areas of Advance Nano and Materials Science.
REFERENCES:
[1] R. Matthias Geilhufe. “Dynamic electron-phonon and spin-phonon interactions due to inertia”. In: Physical Review Research 4.1 (2022), p. L012004.
[2] Friedrich W. Hehl and Wei-Tou Ni. “Inertial effects of a Dirac particle”. In: Physical Review D 42.6 (1990), p. 2045.

SUPERPARAMAGNETIC IRON OXIDE NANOPARTICLES AS DUAL FUNCTIONAL T1 AND T2 CONTRAST AGENTS FOR ENHANCE MAGNETIC RESONANCE IMAGING

Hamza Yakubu, Alexandra Stubelius
Department of Life Sciences, Chalmers University of Technology, Gothenburg, Sweden

INTRODUCTION: Imaging cancer cells is crucial for accurate diagnosis, and Magnetic Resonance Imaging (MRI) offers a non-ionizing imaging modality. However, current gadolinium-based contrast agents, which enhance MRI image quality, are associated with toxicity concerns, including nephrogenic systemic fibrosis (NSF), gadolinium deposition in the brain, and potential nephrotoxicity prompting the search for safer alternatives [1]. Superparamagnetic Iron Oxide Nanoparticles (SPIONs) are promising due to their biocompatibility and unique magnetic properties [2]. This study focuses on developing monodisperse SPIONs (nanocubes, nanospheres, and nanostars) using the solvothermal method [3]. The nanoparticles were functionalized with dopamine to create biocompatible and functional dual T1 (bright signal) and T2 (dark signal) contrast agents for enhance Magnetic Resonance Imaging of tumour cells, offering a safer alternative to gadolinium-based agents.

METHODS: SPIONs were synthesized via the solvothermal method, adapting the approach reported by Gavilán et al. [3]. Briefly, a homogeneous solution of 1-octanol, hexadecyl amine, and oleic acid was prepared in a glass vial under magnetic stirring (1000 rpm) at 60°C for 30 min. After cooling to room temperature, iron pentacarbonyl and benzaldehyde were added, and the mixture was stirred (1000 rpm) for 30 min. The solution was then transferred to a 25.0 mL solvothermal autoclave reactor and heated at 200°C for 4 h. By varying the ratio of benzaldehyde (shape-directing agent) to iron pentacarbonyl, nanoparticles with different shapes were achieved.

RESULTS: The synthesis of nanoparticles with distinct shapes was achieved by adjusting the ratio of iron pentacarbonyl to benzaldehyde. Ratios of 1:0.6, 1:0.4, and 1:0.2 yielded nanostars, nanocubes, and nanospheres, respectively (Figure 1). This approach demonstrates the importance of controlling reaction conditions to tailor nanoparticle

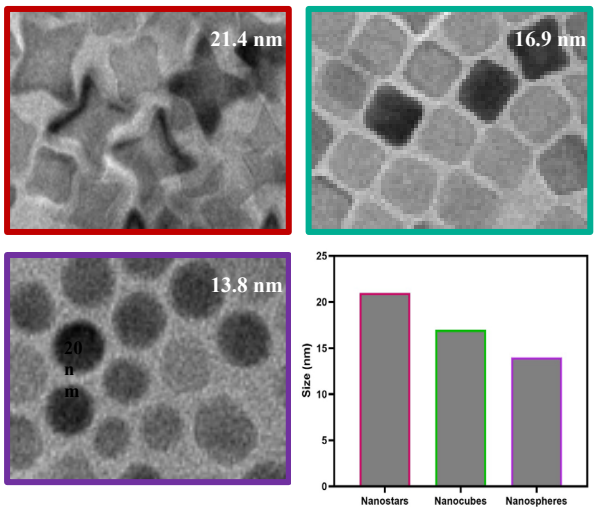

Fig 1: *TEM images of iron oxide nanoparticles including Nanostars, Nanocubes, Nanospheres and their sizes.*

DISCUSSION & CONCLUSIONS: Iron oxide nanoparticles of different shapes such as nanocubes, nanostars and nanospheres were synthesized. The surface of the nanoparticles was functionalised with dopamine to enhance their biocompatibility.

ACKNOWLEDGEMENTS: The authors would like to thank Chalmers Area of Advance Nano for financial support.

REFERENCES:

1. Jeon M, et al., (2021), Adv Mater

2. Yung-Kang Peng, et al., (2016), Materials Today.

3. Gavilán, H., et al. (2023). Nat Protoc.

3D Printed Yeast-Based Materials for Sustainable Architecture

Z. Hefny [a], Y. Bektas [b], E. Orzan [c], M. Zboinska [b] and C. Geijer [a]

a Department of Life Sciences (LIFE), Chalmers university of technology

b Department of Architecture and Civil Engineering (ACE), Chalmers university of technology

c Department of Chemistry and chemical engineering, Chalmers, Sweden

Email: zeinab.hefny@chalmers.se

INTRODUCTION: The integration of biological systems into architectural materials offers a promising path toward sustainable construction (Sandak, 2023). Yeast are versatile microorganisms that are currently being explored in various biotechnological applications. This study investigates the development of 3D printed yeast-based materials that combine structural functionality with biological activity to address sustainability challenges in architecture.

METHODS: A range of materials and strains were tested to identify optimal conditions for embedding yeast cells while maintaining their viability. Experimental setups included variations in material matrix composition and yeast strains. Viability tests were conducted over a 21-day period. The study explored how different components, including glycerol, chitin, and calcium carbonate, impact the mechanical properties and microstructural characteristics of the biomaterial and yeast viability.

RESULTS: The results demonstrate that yeast cells embedded in specific 3D printed matrices remain viable for at least 30 days post-fabrication. Moreover, the structural integrity of the printed materials was maintained, highlighting their potential for dual functionality as both construction material and biologically active substrate.

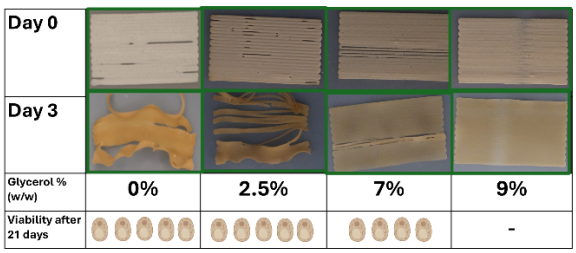

Fig. 1: Glycerol at 7 % (w/w) improved flexibility and prevented cracking and yeast cells remained viable for 21 days.

DISCUSSION & CONCLUSIONS: This study establishes the feasibility of incorporating living yeast into 3D printed materials for sustainable architectural applications. The findings pave the way for further research into bio-integrative construction technologies, offering innovative solutions for environmentally friendly building practices.

ACKNOWLEDGEMENTS: This work is supported by the Energy Area of Advance at Chalmers University of Technology.

REFERENCES: Sandak, A. (2023). Engineered living materials for sustainable and resilient architecture. Nature Reviews Materials, 8(6), 357-359. https://doi.org/10.1038/s41578-023-00554-0

Understanding Species-Dependent Behavior of Mycelium Fibers in Aqueous Suspensions: Composition, Dispersion, and Morphology

L. Zha[1,2], C. Rantzos[1,2], A. Jiménez Quero[1,2]

[1]*Division of Industrial Biotechnology, Department of Life Sciences, Chalmers University of Technology, Gothenburg, SE* [2] *Wallenberg Wood Science Center, Gothenburg, SE*

INTRODUCTION: Mycelium fibers, derived from fungal biomass, represent an emerging class of bio-based building blocks for sustainable materials. Unlike traditional cellulosic fibers from wood or other plants, which are extensively characterized and industrially optimized, the structural and interfacial behavior of mycelium-derived fibers remains largely unexplored. These fibers are inherently composite in nature, containing polysaccharides, proteins, and other extracellular components, which impart distinct surface chemistry and network-forming abilities. This study aims to elucidate how species-dependent biochemical composition governs the dispersion stability and morphological characteristics of mycelium fibers in aqueous systems, thereby establishing the fundamental understanding for their rational use in bio-based material design.

METHODS: Mycelium from three fungal species, *Ganoderma lucidum*, *Fomes fomentarius*, and *Pleurotus ostreatus*, was cultivated in liquid culture, harvested and freeze-dried, and finally resuspend in water as fiber suspension. The fibers were characterized using Fourier-transform infrared spectroscopy (FTIR), elemental analysis and monosaccharides profiling to determine biochemical composition. Dispersion stability was evaluated through zeta potential measurements and optical monitoring of colloidal behavior across pH 2-10. Microscopic analyses, including optical, and scanning electron microscopy, were employed to examine fiber morphology and network organization.

RESULTS: The three fungal species exhibited distinct compositional and interfacial characteristics that influenced their dispersion behavior. Across the tested pH range, all samples showed a transition from positive to negative zeta potential, with isoelectric points located between pH 2 to 4. *G. lucidum* presented the broadest variation in zeta potential, shifting from approximately +10 mV to below −30 mV, while *F. fomentarius* and *P. ostreatus* displayed narrower and less negative potential profiles. This broader range for *G. lucidum* corresponds to its higher content of ionizable polysaccharides and surface-associated biomacromolecules.

In terms of fiber morphology, the fiber diameters of all three species were comparable. However, *G. lucidum* produced the most well-defined fibers, characterized by a high aspect ratio and frequent branching. *F. fomentarius* exhibited the least branched and more linear fibers, while *P. ostreatus* generated shorter fibers with moderate branching.

DISCUSSION & CONCLUSIONS: The comparative analysis reveals that mycelium fibers differ markedly in their surface charge behavior, dispersion stability as well as fiber morphology depending on fungal species. The pronounced pH-dependent charge response of *G.lucidum* highlights the influence of its biochemical composition, particularly its abundance of amphoteric surface groups, in defining aqueous interfacial properties. These results demonstrate that mycelium fibers, with their composite biochemical nature, exhibit surface chemistries fundamentally distinct from traditional lignocellulosic fibers. Understanding these species-dependent behaviors provides essential insight for tailoring mycelium-based fibers as stable, functional building blocks in future bio-based material systems.

ACKNOWLEDGEMENTS: The authors acknowledge funding from the Knut and Alice Wallenberg Foundation (KAW) through the Wallenberg Wood Science Center (WWSC 3.0: KAW 2021.0313).

Rational design of degradable polymers for transient electronics

V. Maruzzo[1], R. Bicudo Ribeiro[1], L. Franco[1], K. Kotewicz,[1] and E. Wang[1]

[1]*Department of Chemistry and Chemical Engineering, Chalmers University of Technology, Göteborg, SW*

INTRODUCTION: Electronic wastes contribute significantly to global pollution, and end-of-life treatments can be environmentally expensive.[1] Thus, the development of transient electronics, designed for controlled degradation and recyclability, is a critical goal for sustainable materials development.[2] In this communication, we explore how the electronic density within imine bonds impact the degradation rate of imine-containing organic semiconductors. By understanding the correlation between molecular motif and degradability, future conjugated polymers can be designed more adequately to ensure a good performance/end-of-life balance.

METHODS: A series of imine-containing small molecules was obtained by condensation of aromatic primary amines (or nitro compounds, reduced *in situ*) and aromatic aldehydes. Either electron withdrawing (benzothiadiazole and thiazole), donating (thiophene) or neutral (benzene) scaffolds were selected, to efficiently modulate the electronic density on the imine bond and consequently its degradability (*figure 1*). Degradation kinetics were followed by UV-VIS spectroscopy: the small molecules were solubilized in THF (3 x 10^{-5} M), and the absorbance was monitored over time upon the addition of a variable amount of trifluoroacetic acid (TFA), in the presence of water. First-order kinetics were observed for all the molecules, evidenced by hypsochromic shift of absorbance during time, consistent with the structural changes expected in the conjugated system.

RESULTS: Degradation studies showed substantial differences among the small molecules. When the imine bond is flanked by electron donating scaffolds (such as in the case of TIT, thiophene-C=N-thiophene), the lowest degradation rate was observed, while higher degradation rates were found for molecules featuring neutral or electron withdrawing units (such as for BIB, benzene-C=N-benzene, and BTIB, benzothiadiazole-C=N-benzene) (*table 1*). Computational investigations are currently ongoing for a comprehensive interpretation of the observed experimental trend.

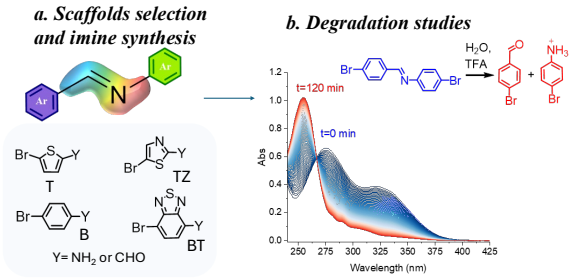

Fig. 1: a) Aromatic units employed for the synthesis of degradable molecules and b) absorbance over time during BIB degradation experiment in THF with 100 equivalents of TFA 7 M.

Table 1. Half-life ($T_{1/2}$) of BIB, BTIB and TIT in presence of different amount of TFA 7 M.

	$T_{1/2}$ (500 eq. TFA)	$T_{1/2}$ (1000 eq. TFA)
BIB	8 min	4 min
BTIB	2 min	0.5 min
TIT	7400 min	3300 min

DISCUSSION & CONCLUSIONS: The electronic distribution strongly affected the degradability of the small molecules, demonstrating the importance of a strategic scaffold selection when designing degradable semiconductors for transient electronics. The small molecules will be implemented through Stille coupling in conjugated polymers, whose degradability will be assessed to establish structure–degradability relationships at the polymer level.

ACKNOWLEDGEMENTS: The authors acknowledge the Swedish Research Council Formas (2023-01008), the Swedish Research Council (2020-05223), the Swedish Energy Agency (P2021-90067), and the Wallenberg Foundation (2022.0192) for financial support. Computations were performed at NSC Tetralith provided by the National Academic Infrastructure for Supercomputing in Sweden (NAISS) funded by the Swedish Research Council through grant agreement no. 2022–06725 (NAISS).

REFERENCES: 1. K. Liu, *et al.*, Circular Economy, 2 (2023), 100028. 2. A. Uva, *et al.,* J. Am. Chem. Soc., 146 (2024), 12271.

Towards Sustainable Electronics: Combining Conducting Polymers with Biopolymers, and Chemically Tuning the Solubility.

Mathis. M. Brette[1], Birhan. A. Abdulahi[1], Leandro. R. Franco,[1] Ergang. Wang[1]

[1]*Chalmers University of Technology, Department of Chemistry and Chemical Engineering, Gothenburg, Sweden*

INTRODUCTION:

As the efficiency of organic-based electronics rises over the years, so does the issue of processing the materials present in their active layer. With the initial aim of synthesizing an ethanol-soluble polymer, a simple water-soluble polymer, or poly(3-esterthiophene-ethylene glycol-random-carboxylic acid thiophene) (P3EGT-rCAT) was made using self-direct arylation polymerization. This polymer was synthesized in only 3 steps and is soluble in 100% water as well as a mixture of 85v% water/EtOH. [1]

Following a different strategy, we aimed to combine the high efficiency of a well-established conducting polymer, polybenzodifuranone, together with the bioavailable lignin sulfonate. With their respective high redox activity, their specific performance was measured for supercapacitors and compared with PEDOT:PSS, and PEDOT:F two state-of-the-art conducting polymers. [2]

METHODS:

P3EGT-rCAT is hydrophilic under neutral/alkaline conditions, but hydrophobic under acid ones. Films spin-coated using water can also be neutralized later to achieve hydrophobicity for further application. Due to the nature of the reaction condition, potassium ions are either acting as counter ions to the carboxylate part of the polymer or being chelated by the glycol and ester group of the polymer. The optical, thermal, and electrochemical properties of P3EGT-rCAT will be compared against P3HT.

For supercapacitor application, freshly synthesized polybenzodifuranone (PBDFO) was combined with lignin sulfonate and the specific capacitance was compared to PEDOT:PSS and PEDOT.

RESULTS: Films of P3EGT-rCAT can be processed from water and stabilized in citric acid. This novel polymer will then be applied and characterized in devices such as OPVs, OECTs/OFETs, ETL, OLECs, and so on.

For the second strategy, the specific capacitance using 6:6:1 weight ratio PBDFO/lignin/Kuraray went as high as 186 F/g compared to 17.2 F/g and 12.2 F/g for PEDOT:PSS and PEDOT:F respectively.

DISCUSSION & CONCLUSIONS:

P3EGT-rCAT is the first one-step polymer with partial side-chain cleavage, allowing for strong water affinity. This affinity can be tuned by pH for bioelectronics.

PBDFO is shown to be compatible with the readily bioavailable lignin sulfonate and can be used as supercapacitor.

ACKNOWLEDGEMENTS: This project is financed by the WISE Knut and Alice Walenberg foundation.

REFERENCE:

(1) Tseng, H.-S.; Puangniyom, T.; Chang, C.-Y.; Janardhanan, J. A.; Yu, H.; Chen, W.-C.; Chueh, C.-C.; Hsiao, Y.-S. Strategically Tailoring Ethylene Glycol Side Chains with Bridged-Carbonyl Ester in Polythiophene-Based Organic Electrochemical Transistors for Bioelectronics. *Chemical Engineering Journal* **2024**, *486*, 150371. https://doi.org/10.1016/j.cej.2024.150371.

(2) Genene, Z.; Xia, Z.; Yang, G.; Mammo, W.; Wang, E. Recent Advances in the Synthesis of Conjugated Polymers for Supercapacitors. *Adv Materials Technologies* **2024**, *9* (9), 2300167. https://doi.org/10.1002/admt.202300167.

3D Bioprinting of Yeast Bioreactors Using Optically Active Nano-Cellulose

A. Mishra[1], S. Muñiz-Calvo[2], K. Sekar[1], V. Ghai[1], V. Siewers[2], M.Chandregowda[1], P. Santosh[2], I. Mijakovic[2], R. Kádár[1]

[1]*Chalmers University of Technology, Department of Industrial and Materials Science, Göteborg, 41296, Sweden*

[2] *Chalmers University of Technology, Department of Life Sciences, Göteborg, 41296, Sweden*

INTRODUCTION: Cellulose nanocrystals (CNCs) are renewable, biocompatible nanomaterials that can form hydrogels with tunable rheology, optical birefringence, and network-forming capability, that make them attractive for extrusion-based 3D bioprinting. Here, CNC was explored as a novel bioink scaffold for printing and culturing yeast cells, with potential applications in biocatalysis and biosensing.

METHODS: CNC suspensions were characterized rheologically to optimize concentration and flow properties suitable for extrusion printing. To explore the viability of the yeast cells, *Saccharomyces cerevisiae* strain CEN.PK 113-7D with or without expression of green fluorescent protein (GFP) were cultured in a media containing yeast nitrogen base and glucose to ensure the necessary nutrients for yeast growth, and then homogeneously mixed with 10 wt% CNC hydrogels. Bioprinting trials were performed at different extrusion pressures and printing velocities to determine optimal conditions for filament continuity and structural fidelity. The printed constructs were incubated under controlled conditions, and cell viability was monitored over five days by colony-forming unit (CFU) assay and microscopy.

RESULTS: The CNC bioink displayed strong shear-thinning and rapid recovery behavior, enabling stable 3D printing at moderate pressures. Its intrinsic birefringence provided a non-invasive optical signature for monitoring structure integrity. Yeast cells remained viable post-printing and proliferated within the CNC network, showing an increase in cell viability by nearly two orders of magnitude over three days before plateauing.

DISCUSSION & CONCLUSIONS: These findings demonstrate that CNC hydrogels provide both mechanical support and a biocompatible microenvironment for yeast cell growth. Their optical activity adds functionality for visualization and monitoring. The combination of structural fidelity, biocompatibility, and metabolic activity establishes CNC as a promising material for biofabrication and as a scaffold for yeast-based living material platform.

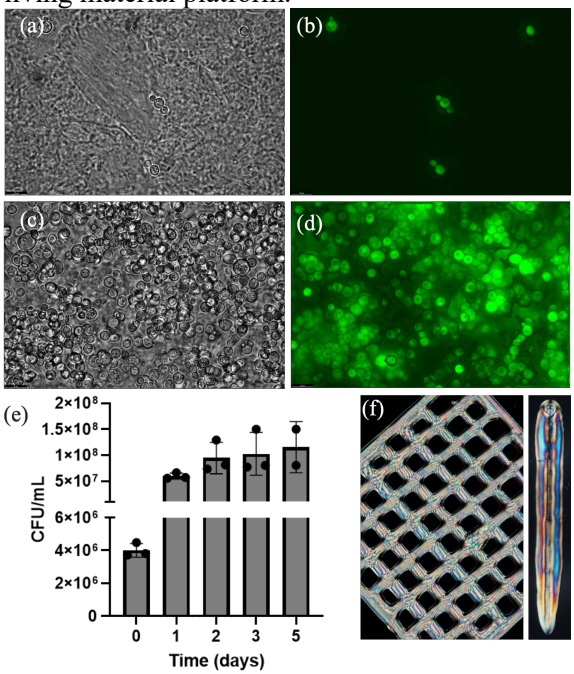

Fig. 1: Brightfield (a-c) and fluorescence (b-d) microscopy of cell growth in bioprinted structure on day 0 (a-b) and day 3 (b-d), at 100X magnification. (c) Cell viability of yeast cells over 5 days. (f) Bioprinted sample exhibiting birefringence.

ACKNOWLEDGEMENTS: This project has received funding from the European Union's Horizon 2020 research and innovation programme under the Marie Skłodowska-Curie grant agreement No 955605. RK and VG are grateful for the financial support of the 2D-TECH Vinnova Competence Centre (Ref. 2019-00068), and Chalmers Area of Advance. SP is grateful to Vetenskapsrådet (2020-04096) and VINNOVA (2023-04134) for their financial support. VS and SMC are grateful to Vetenskapsrådet (2021-05638_VR) for financial support. KS and RK thank WWSC for their financial support

Laser Additive Manufacturing of High Silicon Steel Soft Magnetic Materials

M. Murali[1], E. Hryha[1], U. Klement[1], V. Chaudhary[1]

[1]*Centre for Additive Manufacture-Metal (CAM[2]), Department of Industrial and Materials Science, Chalmers University of Technology, Sweden*

INTRODUCTION: Soft magnetic materials play a crucial role in enhancing the efficiency of electric motors, which are becoming increasingly important in the era of electric transportation. While traditional Si steel (Fe-3.2 wt.% Si) performs well in low frequencies, it shows limitations at higher frequencies, promoting the search for alternative materials[1]. High silicon steel alloys, with 6.5% silicon content present a promising alternative due to their high electrical resistivity, low iron loss, and minimal magnetostriction, rendering them well-suited for mitigating energy losses, failures, and noise commonly encountered in high-frequency environments [2]. However, the brittleness inherent to high silicon steel alloys presents manufacturing challenges during conventional processing techniques. The study explored the feasibility of using the Powder Bed Fusion- Laser Beam (PBF-LB) additive manufacturing (AM) technique to produce Fe-6.5wt%Si soft magnetic materials with enhanced multi-properties for high-frequency electric machines.

METHODS: Gas-atomized Fe-6.5wt.%Si powder (10-50 µm) provided by Höganäs was used as feedstock material. Cubes of 5*5*5 mm3 were printed using PBF-LB EOS M100 machine employing DoE-based process parameter optimization within a Volumetric Energy Density (VED) range of 30 to 210 J/mm3. Microstructure and crystal structure were analyzed using a Gemini 450 FEG-SEM and a Bruker AXS D8 advanced diffractometer, respectively. The magnetic properties were measured using a Lakeshore 8600 Series Vibrating Scanning Magnetometer (VSM).

RESULTS AND DISCUSSION: The samples printed with a VED above 100 J/mm3 exhibit a relative density higher than 95%. Below 100 J/mm3 the samples exhibit a higher volume of lack of fusion porosities and above 150 J/mm3 keyhole porosities are dominant. Within this range (110-145 J/mm3), cracks hinder achieving fully dense samples. Using laser power (P) in the range of 125-150 W and scan speed(S) in the range of 800-1000 mm/s, with a fixed layer thickness (T) of 20 µm and hatch distance (H) of 60 µm, samples are printed with a maximum relative density of 98.6%. Cross-sectional analysis reveals numerous vertical cracks parallel to the build direction. Solidification microstructure analysis indicates intergranular and intercellular crack propagation, suggesting multiple mechanisms involved in the cracking. Further studies are needed to understand the cracking mechanisms. The magnetic properties measured on as-build samples with a relative density exceeding 98%, exhibit saturation magnetization (Ms) ranging from 201 to 217 emu/g and coercivity (Hc) from 0.96 to 1.34 Oe. The sample with a VED of 116 J/mm3 (P=140W, S=1000mm/s, T=20µm and H=60µm) exhibited an Ms of 217 emu/g and an Hc of 1.34Oe. On the other hand, lower values of Ms, 201 emu/g, and Hc, 0.96 Oe, were measured for the sample printed with a VED of 120 J/mm3 (P=130W, S=900mm/s, T=20µm and H=60µm).

CONCLUSIONS: Fe-6.5wt%Si alloy samples were printed using the PBF-LB process. The magnetic properties and relative density of as-built samples are significantly influenced by AM process parameters. Samples with relative density > 98% exhibit a high saturation magnetization and low coercivity. However, challenges such as crack formation remain significant in achieving fully dense samples, requiring further investigation to optimize the process parameters and microstructure. This study highlights that materials with high silicon content such as Fe-6.5Si, can be produced with attractive magnetic properties through precise adjustment of process parameters in PBF-LB.

ACKNOWLEDGEMENTS: The work is supported by the Area of Advance (AoA) Production and Materials Science at Chalmers and Centre for Additive Manufacture-Metal (CAM2), Chalmers University of Technology.

REFERENCES:

[1] Varahabhatla, Saisree Meenakshi, et al. Influence of energy density on the microstructure, growth orientation, and

Nanocellulose for Sustainable Decoy

P. Luts[1], C. Gullström[1], H. Kariis[1]

[1]*Swedish Defence Research Agency (FOI)*

INTRODUCTION: In the pursuit of misleading the enemy, decoys that imitate real military targets present a wide variety of uses. This master's thesis investigated the potential of using nanocellulose as a sustainable decoy material, designed to mimic a nylon tent within a spruce forest background.

METHODS: The nanocellulose samples consisted of cellulose nanofibril (CNF), glycerol, deionized water, and varying amounts of a mixture consisting of chromium oxide green (COG) pigment and deionized water. The samples were dried using and oven and then compared with a nylon tent fabric and spruce by means of scatterometry and spectrometry measurements, as well as uniaxial tension tests.

RESULTS:

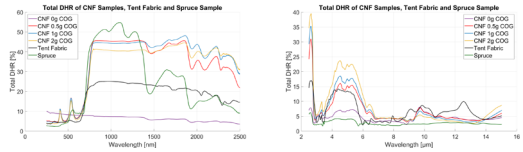

Fig. 1: Total directional hemispherical reflection (DHR) of CNF samples, tent fabric, and spruce sample in the range 250–2500 nm (left) and 2.5–15 µm (right).

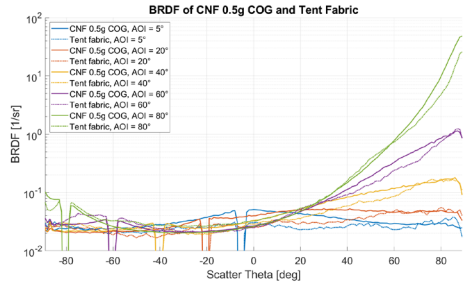

Fig. 2: Bidirectional reflection distribution function for one CNF sample containing 0.5g COG mixture and the tent fabric at 633 nm for different angel of incidence (AOI).

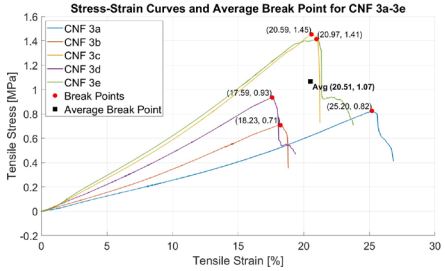

Fig. 3: Uniaxial tension test performed on CNF samples.

DISCUSSION & CONCLUSIONS:
The results indicated that the CNF sample containing 2g COG mixture most closely replicates the tent's total DHR in the range 250–1000 nm, while the sample with 1 g of COG mixture provided the best match in the 1000–2500 nm range. In the 2.5–15 µm region, the CNF sample containing 0.5 g of COG mixture exhibited the closest replication to the tent fabric.

The scatterometry measurements indicated that at 633 nm, the tent fabric and CNF 0.5g exhibit similar behaviour. Both samples display diffuse reflection, distributing light uniformly, with increasing levels of both forward and back scattering observed as the angle of incidence (AOI) increases.

The average tensile stress at breakage was 1.1 MPa with a standard deviation of 0.3 MPa. The average tensile strain was 21 % with a standard deviation of 3 pp. The tent fabric had an average tensile stress at breakage of 125 MPa with a standard deviation of 5 MPa, and an average tensile strain at breakage of 27 % with a standard deviation of 0.9 pp. These results suggest that the tent fabric and the CNF samples exhibit similar elasticity, however, the tent fabric demonstrates significantly higher strength than the CNF samples.

The nanocellulose samples did not fully resemble the mechanical and optical properties of the tent fabric. However, the samples demonstrated potential in certain wavelength regions, particularly within the UV-VIS and 2.5–15 µm ranges. With further modifications, the material could potentially be utilized for decoy purposes, such as to resemble a tent fabric.

Density functional study of coating on magnesium implants

Miranda Naurin, Anthony Veit Berg, Elsebeth Schröder

Department of Microtechnology and Nanoscience (MC2), Chalmers

INTRODUCTION: Orthopedic implants are commonly made from metals such as titanium and stainless steel, but their stiffness can cause stress shielding and sometimes require removal as they are not biodegradable. An alternative is biodegradable magnesium (Mg) implants if the rapid corrosion of Mg can be impeded. We study coating of Mg surfaces using density functional theory (DFT).

METHODS: DFT calculations are carried out to investigate magnesium hydroxide ($Mg(OH)_2$) and hydroxyapatite (HAp) coatings on Mg(0001) surfaces. We obtain the adsorption energy of the coating from the difference in total energies for the Mg-surface (s), the individual coatings (m) and the combined system (s+m)

$$E_{ads} = E_{s+m} - E_s - E_m. \qquad (1)$$

We test for preferred relative position of the coating relative to the Mg surface atoms. We further study the adsorption of body-relevant amino-acids on the coating, and how alloying of the Mg-surface with Zn and Ca affect the binding of the coating to Mg.

RESULTS: By testing 25 different adsorption positions for each coating, we see that both HAp and $Mg(OH)_2$ have a preferred binding position on the Mg-surface. The optimal coating adsorption energies (1) are listed in Table 1. However, other positions (obtained by sliding the coating along the Mg surface) have only slightly different adsorption energies. This shows that both coatings tend to slide laterally on the Mg surface.

Structural changes of surfaces, coatings and adsorbed molecules were observed after adsorption. Two examples are shown in Fig. 1. We find that amino acids, present in the body, bind to the $Mg(OH)_2$ coating, likely improving the integration of the implant into the body.

Table 1. Calculated adsorption energies.

System	Energy (meV/Å^2)
$Mg(OH)_2$-Mg	-15.8
HAp-Mg	-12.5
HAp-Mg-Zn	-19.4
HAp-Mg-Ca	-18.4

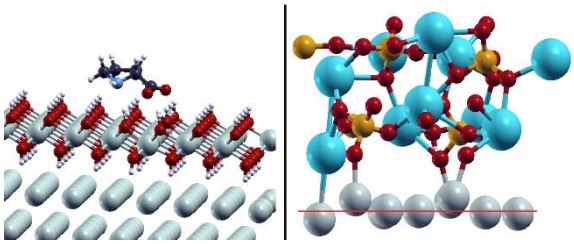

Fig. 1: Optimized structures. Proline over $Mg(OH)_2$ surface (left);. HAp over Mg-surface (right). Visualized using XCrySDen

Our calculations show that the binding improves when the Mg surface is doped with Zn or Ca, and with a single Ca atom at a certain position relative to HAp a possible crack formation is indicated.

DISCUSSION & CONCLUSIONS: The adsorption energies and structural changes have been obtained by use of DFT calculations. They indicate that HAp and $Mg(OH)_2$ bind to the Mg surface with a relatively low energy (lift off possible) and with little energy required for sliding along the Mg surface (low corrugation, sliding off possible).

All calculations are performed in vacuum, which means that many environmental parameters are not included. Our next step is to calculate the electron charge density which will allow us to analyse how electrons are distributed between the coatings and the Mg-surface.

ACKNOWLEDGEMENTS: This work is partially based on student reports involving also the following Chalmers students: Sally Aldhaim, Moltas Elliver, Ablai Forster, Ludwig Hagby, Tim Hansson, Alexandra Jernstedt, Didrik Nilsson, and Emmy Salminen.

Work supported by Chalmers Area of Advance (AoA) Nano and AoA Materials, the Swedish National Science foundation (VR2020-04887), the National Academic Infrastructure for Super-computing in Sweden (NAISS2024/3-16, NAISS2024/6-432 and NAISS2025/5-484) and by Chalmers Centre for Computational Science and Engineering (C3SE).

Artificial Nuclear Pore Complexes with Highly Selective Shuttle-Cargo Transport

J. Medin[1,†], B. Santoso[1], L. Beckerman[2], Radhika Vattikunta[1], Rebekah Hailes[1], John Andersson[1], Andreas Dahlin[1].

† jmedin@chalmers.se
1 Department of Chemistry and Chemical Engineering, Chalmers University of Technology
2 Department of Physics, Chalmers University of Technology

The nuclear pore complex (NPC) is a large protein assembly situated at the nucleoporins that perforate the nuclear envelope, the double membrane that encloses the nuclear genome of a cell and separates the nucleus from the cytoplasm. The NPC regulates transport of biomolecules to or from the nucleus, and it is capable of facilitated transport where "cargo" species can bind to "shuttles" which specifically translocate the nucleoporins, while the "cargo" cannot pass alone[1]. In order to better understand the transport mechanism of the NPC, several attempts have been made to reconstruct the NPC transport using synthetic systems. However, it has proven difficult to achieve a functioning shuttle-cargo transport mechanism, in particular with high selectivity.

In the last few decades, research on antifouling materials have made it relatively easy to design a system that denies macromolecules, such as proteins and large polymers, access to a surface. One prominent solution to the fouling problem is the use of polymer brushes: polymers attached to a surface densely enough to promote stretching of the polymers once exposed to a solvent into a "brush" structure[2]. These brushes are known to prevent all macromolecules larger than a ~2 kDa from entering the hydrated structure, while allowing small molecules such as water and ions to freely diffuse through them[3]. However, it is a different story to imagine a similar system that rejects most macromolecules while allowing certain macromolecules access.

In this work, we present a fully artificial NPC transport mechanism based on hydrogen bond complexation between hydrophilic polymers consisting of poly(*N*-hydroxyethyl acrylamide) and polyelectrolyte shuttles consisting of poly(methacrylic acid). At low pH, multivalent bonds between the two polymers enable selective and fast transport of this polymer through the brush barrier without strongly altering its morphology. Furthermore, as a mimic of nucleic acid export through the NPC, we show that cargo strands conjugated to the shuttles translocate through the pores even though they are too large to pass otherwise. Overall, the selectivity of our system is much better than what has been previously demonstrated for artificial systems and even better than the real NPC, the pH-responsive nature of our system enables applications such as trapping of molecules in nanoscale chambers or any application where triggered transport is of interest.

This work is currently available as a preprint on ResearchGate. Search for "Artificial Nuclear Pore Complexes with Highly Selective Shuttle-Cargo Transport". Released June 2025.

(1) M. Beck and E. Hurt (2017). Nature Molecular Cell Biology **18**(2): 73
(2) Chen, W., et al (2017). Macromolecules **50**(11): 4089.
(3) Medin, J., et al (2025). ACS Applied Bio Materials **8**(5): 4008

Zap! Crackle! React! - Towards the Development of Efficient Polymeric Electrodes for Electrosynthesis

R. S Raju, J. Vasquez, M. M. Westwood, A. Giovannitti
Division of Applied Chemistry, Department of Chemistry and Chemical Engineering
Chalmers University of Technology, 412 96 Gothenburg

INTRODUCTION: Electrifying chemical reactions is a promising approach for reducing the carbon footprint of the chemical industry. A key reaction relevant to industrial processes such as drug and fertiliser production, is reductive amination. Copper based electrodes have shown high selectivity for reductive amination reactions [1] along with carbon-based electrodes which also exhibit promising performance due to their conductivity and stability. In this context, conjugated polymers emerge as an intriguing class of materials because of its potential to undergo volumetric charging which could enhance both selectivity and efficiency. Polymeric Organic Semiconductors (OSCs) have tunable electrochemical properties and offer efficient electron transfer reactions [2]. They are formed by connecting repeat units containing alternating single and double bonds (π-conjugated systems). By preparing electrodes based on polymeric OSCs, we aim to surpass the limitations of traditional surface-limited electrodes and develop bulk-active polymeric electrodes that can access reactive sites throughout the volume of the material.

METHODS: I investigate bulk activity of different polymeric OSCs developed in the Giovannitti Group. To understand and optimise bulk-active polymeric electrodes for reductive amination, we need to understand how these materials interact with the electrolyte, reagents and products. Electrochemical Quartz Crystal Microbalance (EQCM) will be used for monitoring mass changes at the electrode surface in real time with nanogram sensitivity. Organic electrochemical transistors (OECTs) measurements are employed to measure changes of the electronic conductivity during electrode operation. They allow us to compare different polymer structures to identify those with optimal ionic-electronic coupling, which is key for achieving high selectivity in reductive animation. This study provides new insights into the role of volumetric charging in electrosynthesis and paves the way for more efficient, selective, and scalable electrochemical routes to amine synthesis.

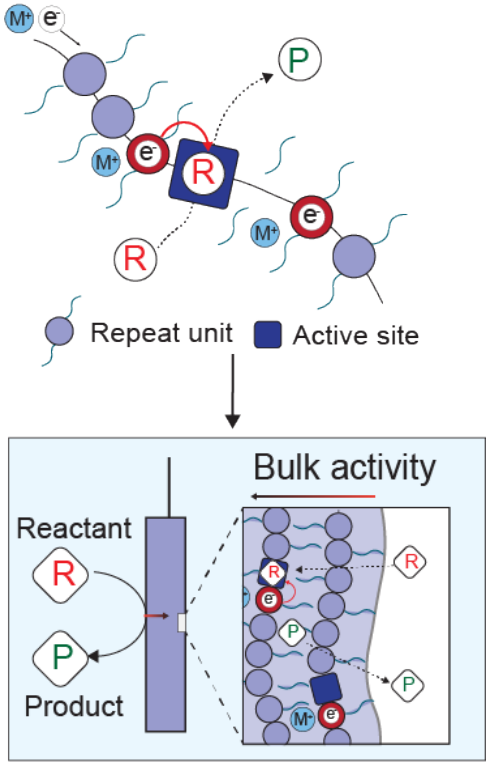

Fig. 1: Simplified illustration of a polymeric OSC with available active sites in the bulk.

ACKNOWLEDGEMENTS: We acknowledge the ERC project (101116071) for supporting this study.

REFERENCES:

[1] Kim, T., Park, D. I., Kim, S., Yadav, D., Hong, S., Kim, S. H., Yoon, H. J., & Jin, K. (2023). Mechanistic investigation of electrocatalytic reductive amination at copper electrode. *Chemical Communications*, *59*(32), 4818–4821. https://doi.org/10.1039/d3cc00296a

[2] De La Fuente Durán, A., Liang, A. Y., Denti, I., Yu, H., Pearce, D., Marks, A., Penn, E., Treiber, J., Weaver, K., Turaski, L., Maria, I. P., Griggs, S., Chen, X., Salleo, A., Chueh, W. C., Nelson, J., Giovannitti, A., & Mefford, J. T. (2023). Origins of hydrogen peroxide selectivity during oxygen reduction on organic mixed ionic–electronic conducting polymers. *Energy & Environmental Science*, *16*(11), 5409–5422. https://doi.org/10.1039/d3ee02102e

Anisotropic nanoparticles vs vortices: a Taylor-Couette-PLI-SAXS study

K. Sekar[1,6], V. Ghai[1], R. Ghanbari[1,2,a], M. Bek[1], M. Liebi[3,4,5], A. Matic[3,6], A. E. Terry[2], K. Nygård[2], R. Kádár[1,2,6]

[1]Department of Industrial and Materials Science, Chalmers University of Technology, Gothenburg, Sweden, [2] MAX-IV Laboratory, Lund University, Lund, Sweden, [3] Department of Physics, Chalmers University of Technology, Gothenburg, Sweden, [4]Division of Photon Science, Paul Scherrer Institute, Villigen, Switzerland, [5]Institute of Materials, Ecole Polytechnique Fédérale de Lausanne (EPFL), Lausanne, Switzerland, [6]Wallenberg Wood Science Center, Chalmers University of Technology, Gothenburg, Sweden, [a]Present address: NKT Technology Consulting, Västerås, Sweden

INTRODUCTION:

Transitions from laminar to turbulent flow proceed via a series of secondary flows with ordered and chaotic vortices across multiple length scales. Taylor Couette (TC) flow is a benchmark setup to study these transitions. Using material's inherent and flow-induced birefringence, polarized light imaging (PLI) was used to capture macroscopic patterns formed by the vortices. In combination with small-angle X-ray scattering (SAXS), we were able to resolve macroscopic pattern formation and their nanoscopic dynamics that have not previously been revealed.

METHODS:

Two anisotropic nanoparticle systems were chosen to study their impact on pattern formation and flow effects on particle dynamics: 1D rod-like cellulose nanocrystals (CNC) and 2D platelet-like Graphene oxide (GO). Experiments were performed in a custom Taylor-Couette cell mounted on a rheometer, enabling flow visulization. An optical train with crossed linear polarizers, LED light source and a DSLR camera was used to capture macroscopic pattern formation via PLI. Two-dimensional fast Fourier Transform were applied to the PLI images to obtain temporal and spatial frequency spectra. Small angle X-ray scattering (SAXS) experiments were conducted at the FORMAX beamline at MAXIV to capture the nanoscopic dynamics across the vortex size.

DISCUSSION & CONCLUSION:

Macroscopic pattern formation captured through PLI revealed that CNC and GO suspensions predominantly followed Newtonian-like behaviour modified by shear-thinning. However, GO shows signs of elasticity at the primary instability transition. At nanoscopic length scales, SAXS frequencies for selected transition flow states of GO aligned with PLI frequencies whereas CNC remained uncorrelated. This suggested at such small length scales, secondary flow effects dominate GO alignment, while CNC is governed by Brownian motion, as characterized by the rotational supercritical-flow Péclet number.

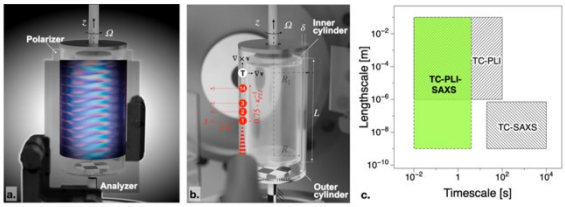

Fig. 1: Custom Taylor-Couette setup for multiscale analysis of nanoparticle suspensions in transitional flow a) PLI setup b) Tangential configuration (T) where SAXS data collected along the vorticity (∇×v) direction

ACKNOWLEDGEMENTS: Research conducted at MAX IV, a Swedish national user facility, is supported by the Swedish Research Council under contract 2018-07152, the Swedish Governmental Agency for Innovation Systems under contract 2018-04969, and Formas under contract 2019-02496. The work was supported by Chalmers Foundation through the project Chalmers Center for Advanced Neutron and X-ray scattering techniques incooperation with MAX IV. K.S., V.G., M.B., and R.K. are grateful for the financial support of the Wallenberg Wood Science Center (WWSC), FibRe Vinnova Competence Center, 2D-TECH Vinnova Competence Centre and Chalmers Areas of Advance Materials Science, Nano and Production.

REFERENCES: Sekar, K. et al., (2025). Multiscale transitional flow in anisotropic nanoparticle suspensions revealed by time-resolved x-ray scatter microscopy. arXiv preprint arXiv:2510.18444.

Unraveling Surface Structure Dynamics on Model Electrocatalysts

F. Simon[1,2], F. Duquet[1,2], G. Abbondanza[1], B. Lönn[1], V. Roth[1], O. Gutowksi[3], A.-C. Dippel[3], B. Wickman[1], U. Hejral[1,2]

[1]Chalmers University of Technology, Gothenburg, Sweden, [2] Wallenberg Initiative for Sustainability, Gothenburg, Sweden, [3]Deutsches Elektronen-Sychrotron P07, Hamburg, Germany

INTRODUCTION: Green hydrogen is key in transforming various industrial sectors towards decarbonization. Non-noble metal electrode materials like Ni, Co and Fe are preferred in alkaline water electrolysis due to their low cost and availability. A major challenge in achieving efficiencies close to the thermodynamic optimum is to overcome the slow kinetics of the oxygen evolution reaction (OER). Moreover, the impact of Fe incorporation on the catalytic properties is not fully understood. Unraveling the correlation between the surface structural dynamics on NiFe electrode systems with the catalytic activity during OER will help the rational design of more efficient electrocatalysts.

METHODS: High-energy surface X-ray diffraction (HESXRD) allows us to monitor the Ni(oxy)hydroxide surface structures in model single crystal Ni(111) electrodes on an atomic scale under operando conditions (Fig. 1).[1] Combining HESXRD with Surface optical reflectance (SOR) gives additional information on optical surface parameters like roughness or chemical composition.[2] Electrodeposition of Fe on Ni(111) enables the investigation of the "Fe-effect" on Ni electrode performance.[3]

RESULTS: Studying HESXRD, SOR and electrochemical data while changing the potential resulted in a correlation between the different features and inflections between the different data sets. We were able to observe a hysteresis during the reduction of the surface between the epitaxial oxyhydroxide vanishing and the hydroxide appearing.

The electrodeposition of Iron improved the efficiency of the Ni electrode and impacted visibly the HESXRD maps with an increased intensity of all features. We found out that the Fe incorporation influences the lattice parameters of the (oxy)hydroxide surface structure.

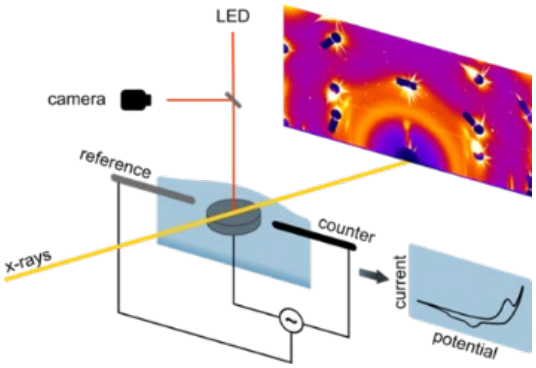

Fig. 1: Illustration of experimental approach combining HESXRD and SOR in an electrochemical cell setup.

DISCUSSION & CONCLUSIONS: We were able to correlate HESXRD, SOR and electrochemical data to identify potential-dependent surface structure transformation processes between Ni(oxy)hydroxides in the transition to OER. Fe doping of the Ni(111) electrode lowered the overpotential required for OER and could be linked to changes in the surface structure. Although SOR is an experimentally simple technique, we found out that it reacts very sensitively to surface changes on Ni.

ACKNOWLEDGEMENTS: We are grateful for the funding from the Wallenberg Initiative for Sustainability (WISE), the Areas of Advance Nano and Energy and the Competence Centre for Catalysis at Chalmers University. The research was supported by the DESY Nanolab in Hamburg.

REFERENCES:

[1] Gustafson, J. et. al. *Science* **2014**, *343*, 758-761

[2] Pfaff, S. et. al. *ACS Appl. Mater. Interfaces* **2021** *13* 19530

[3] Anantharaj, S. et. al. *Nano Energy* **2021**, *80*, 105514